BIOCHEMISTRY
including biophysical chemistry & molecular biology

Article

pubs.acs.org/biochemistry

Inactivation of TEM-1 by Avibactam (NXL-104): Insights from Quantum Mechanics/Molecular Mechanics Metadynamics Simulations

Jacopo Sgrignani,[†,#] Giovanni Grazioso,[‡,#] Marco De Amici,[‡] and Giorgio Colombo*[,†]

[†]Istituto di Chimica del Riconscimento Molecolare, CNR, Via Mario Bianco 9, 20131 Milan, Italy

[‡]Dipartimento di Scienze Farmaceutiche, Sezione di Chimica Farmaceutica "Pietro Pratesi", Università degli Studi di Milano, Via Mangiagalli 25, 20133, Milan, Italy

Supporting Information

ABSTRACT: The fast and constant development of drug-resistant bacteria represents a serious medical emergence. To overcome this problem, the development of drugs with new structures and modes of action is urgently needed. In this context, avibactam represents a promising, innovative inhibitor of beta-lactamases with a novel molecular structure compared to previously developed inhibitors, showing a promising inhibitory activity toward a significant number of beta-lactamase enzymes. In this work, we studied, at the atomistic level, the mechanisms of formation of the covalent complex between avibactam and TEM-1, an experimentally well-characterized class A beta-lactamase, using classical and quantum mechanics/molecular mechanics (QM/MM) simulations combined with metadynamics. Our simulations provide a detailed structural and energetic picture of the molecular steps leading to the formation of the avibactam/TEM-1 covalent adduct. In particular, they support a mechanism in which the rate-determining step is the water-assisted Glu166 deprotonation by Ser70. In this mechanistic framework, the predicted activation energy is in good agreement with experimental kinetic measurements. Additionally, our simulations highlight the important role of Lys73 in assisting the Ser70 and Ser130 deprotonations. While based on the specific case of the avibactam/TEM-1, the simple protocol we present here can be immediately extended and applied to the study of covalent complex formation in different enzyme−inhibitor pairs.

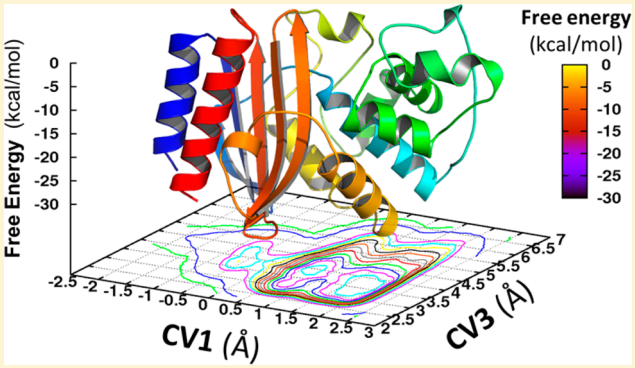

The steady increase in the number of multidrug resistant bacteria is a serious threat for human health worldwide. One of the mechanisms used by Gram-negative pathogens to develop drug-resistance involves the expression of beta-lactamases (BLs), a class of enzymes that hydrolyzes the lactamic ring of common antibiotics such as penicillins, cephalosporins, monobactams, and carbapenems, making them inefficient for bacterial killing.[1−3] BLs have been divided into four subclasses (A, B, C, and D) based on sequence.[4] In class A, C, and D, a serine residue is directly involved in the hydrolytic reaction,[2] while class B enzymes exploit metal cofactors, in particular zinc ions, to carry out the enzymatic hydrolysis of beta-lactamic drugs.[5]

In general, a combination of one beta-lactam drug and one BL inhibitor is commonly employed to overcome resistance to beta-lactam antibiotics. However, the excessive use of these therapeutic combinations, especially in hospital settings, has generated an evolutionary pressure that is accelerating the emergence of resistant bacteria.[1] At present, only three beta-lactam inhibitors (clavulanic acid, tazobactam, and sulbactam) are clinically used against the resistance induced by BL classes A, C, and D, while no inhibitor of class B metal-BL has been approved for therapy. This situation calls for the urgent development of new and potent BL inhibitors for antibiotic therapy.[6,7]

In this context, avibactam (Avi, previously known as AVE1330A or NXL104, Figure 1A) is a new wide-spectrum non-β-lactamic BL covalent inhibitor (Figure 1B) under evaluation in advanced clinical trials (Phase III) for use in combination with the third-generation cephalosporin ceftazidime.[8,9] Avi has been rationally designed to be a true enzymatic inhibitor of BLs with a structure based on a diazabicyclooctane (DABCO) scaffold, different from a classical beta-lactam, thus representing a new molecular entity in the development of antibiotic treatments. In vitro studies have shown that Avi may restore the broad-spectrum activity of cephalosporins against class A, class C, and some class D lactamases.

Thanks to its promising activity combined with its structural novelty, Avi can potentially become the first BL inhibitor brought

Received: May 16, 2014
Revised: July 18, 2014
Published: July 22, 2014

   dx.doi.org/10.1021/bi500589x | *Biochemistry* 2014, 53, 5174−5185

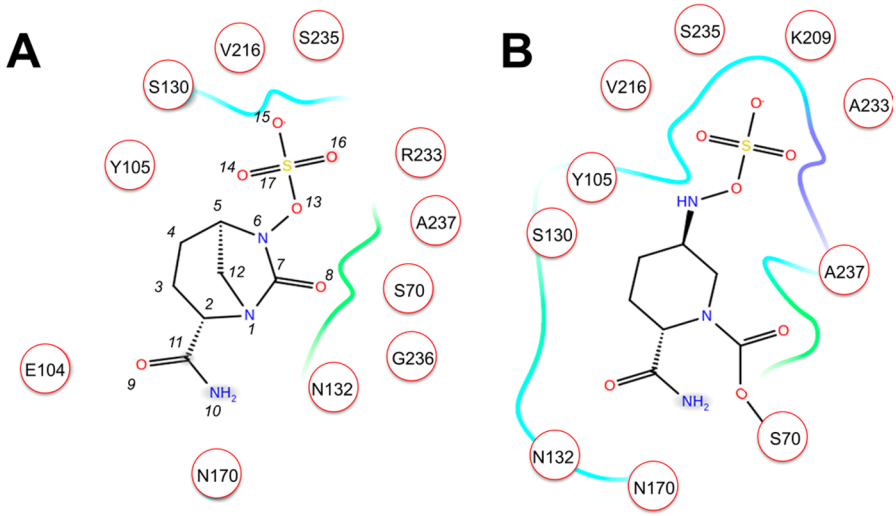

Figure 1. (A) Avi structure in the Michaelis complex with TEM-1 enzyme, (B) TEM-1 in the acylated state. Spheres represent amino acids defining the catalytic site of the enzyme. Atoms belonging to avibactam are numbered for the sake of clarity and immediacy in the discussion of the results.

into common clinical use after 20 years. For all these reasons, extensive work has been carried out to structurally[10,11] and kinetically[9,12,13] characterize the interaction between Avi and BLs from different bacteria. The structures of the inhibitor bound to different BLs revealed similar binding modes.[10,11] Moreover, kinetic characterizations have recently shown Avi to be a reversible, covalent inhibitor.[13]

Prompted by these results and by the potential implications of understanding the inhibition process for the design of new generation antimicrobial agents, we have carried out a series of classical molecular dynamics (MD) and hybrid quantum mechanics/molecular mechanics (QM/MM) simulations with the aim of garnering atomistic insights into the mechanisms of Avi/BL complex formation. At the start of this work, a high resolution protein structure[14] and detailed kinetic data[12] for Avi inhibition were available only for TEM-1, a class A BL (Figure 2).

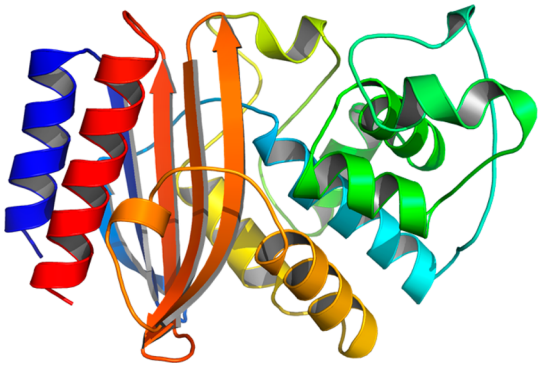

Figure 2. Structural representation of TEM-1.

We thus selected this system as an ideal model to undertake computational investigations of Avi inhibition mechanisms, also considering a number of reported computational studies on the interaction and reactivity of TEM-1 with well-known classical beta lactamic drugs.[15−17]

One of the main goals of the paper was to use a multiscale[18] computational approach to define the structural and dynamic features of the different (putative) intermediates formed along the pathway leading to the formation of the Avi/TEM-1 covalent complex, as well as the differences in free energies among distinct reaction steps and their underlying mechanisms. It must be underlined that our simulations and analyses were limited to this part of the enzymatic cycle. Thus, in the present paper, no mechanistic investigation was carried out on the events following the formation of the covalent intermediate. We have used a combination of approaches ranging from classic molecular mechanics (MM) MD simulations to hybrid quantum QM/MM.[19−27] In particular, we calculated the activation free energy barriers for the different steps necessary for the formation of the Avi/TEM-1 covalent complex using metadynamics (MTD),[28−30] a computational technique designed to enhance the rate of rare events during MD simulations, recently applied also to the study of enzymatic systems.[31−34]

Overall, our results allowed generation of a detailed, atomic-resolution mechanistic model of the structural and energetic determinants of the steps leading to the formation of the Avi/TEM-1 covalent complex. Importantly, the results of the calculations proved to be in good qualitative and quantitative agreement with available experimental data. Specifically, we found overt correspondences with the hypothesis on the reaction mechanism proposed by Docquier and co-workers on the basis of X-ray structure of Avi in complex with one class A and one class C BLs.[11] Our results, combined with those from X-ray structural and in vitro biochemical studies, will contribute to the design of novel derivatives of Avi, opening up the possibility to expand the molecular diversity space of BL inhibitors to overcome resistance phenomena.

MATERIALS AND METHODS

Model System and MD Setup. At the start of our project, no crystal structure of Avi/BL complex was publicly available. The model for the TEM-1/Avi complex was then built starting from the structure of TEM-1/M182T (PDB code 1JWP)[14] in its apo form. Then, Thr182 was mutated into a methionine residue to restore the wild-type enzyme. Notably, Met182 is located far from the catalytic site, and the overall RMSD between our model (1JWP) and 1M40, the X-ray solved structure of TEM-1 with the highest resolution, was only 0.195 Å.

This 1JWP structure was chosen considering that the other available structures solved by X-ray diffraction are cocrystallized with different covalent inhibitors and, consequently, the

dx.doi.org/10.1021/bi500589x | Biochemistry 2014, 53, 5174−5185

conformations of the catalytic sites are adapted to cocrystallized ligands with a chemical structure different from Avi. The protein protonation state was determined using the H++ Web server.[35]

The selected structure was prepared for the simulations through the following steps: (i) the phosphate ions included in the X-ray structure and all the water molecules, except water molecule 346 (Wat-R), postulated to be involved in the enzymatic reaction,[36,37] were deleted. (ii) After structural alignment, Avi was manually placed inside the catalytic site considering the orientation assumed in the X-ray structure of a BL from *Mycobacterium tubercolosis* (PDB code 4DF6).[38] Avi was preliminarily minimized by Gaussian09[39] at the DFT/B3LYP/6-31G(d)[40,41] level of theory. The partial charges of the Avi atoms were assigned with the RESP[42] method and, in accordance with its pK_a, the net charge was set to −1. (iii) The complex was placed in a periodic box large enough to guarantee a minimum distance of 10 Å between the protein and any face of the box. This resulted in a system with about 30000 solvent atoms, and a box volume of 405144 A^3. The TIP3P[43] model was employed to explicitly represent the solvent.

The resulting complex was optimized by molecular mechanics minimization and molecular dynamics (MD) simulations by the *sander* and *pmemd* modules of the AMBER12[44,45] package. *ff12* and *GAFF*[46] force fields were applied for the protein and the ligand, respectively. Neutrality was ensured by rescaling the charges of the α carbon atoms by a factor obtained from the ratio between the system net charge and number of Cα atoms.[47] Considering the superficial position of the catalytic site, and the presence of negatively charged residue, this approach avoided the presence of positively charged ions in close proximity of the reactive center and running simulation with an unrealistic salt concentration.[48−50]

A first minimization step was carried out on water molecules, keeping the atoms of the protein frozen. Then a minimization of the whole system was performed by setting a convergence criterion on the gradient of 10^{-4} kcal mol^{-1} $Å^{-1}$.

Prior to starting the production MD simulations, the system was equilibrated for 40 ps at 300 K in isocore conditions (NVT). Subsequently, a 70 ns of MD simulation in isothermal−isobaric ensemble (NPT) was carried out at 300 K with a 2 fs time-step.

All the simulations were performed in periodic boundary conditions (PBC). van der Waals and short-range electrostatic interactions were estimated within a 10 Å cutoff, whereas long-range electrostatic interactions were assessed using the particle mesh Ewald method.[51]

The SHAKE[52] algorithm was applied to all bonds involving hydrogen atoms. Once the complex model reached equilibration and structural stability (RMSD of protein Cα in the range of 1.5−2 Å), the trajectories were further examined by visual inspection with VMD,[53] thus ensuring that the thermalization did not cause any structural distortion.

QM/MM Calculations. The study of an enzymatic reaction mechanism requires computational methods able to take into account the formation and breaking of covalent bonds in solvated ligand−protein complexes.[19,54,55] Despite recent hardware and software advancements, QM calculations capable of treating a fully solvated biological system at a high level of theory are still too expensive. A common solution to this limitation is the application of mixed QM/MM potential, in which only the residues and solvent molecules involved in the reaction are simulated at the QM level, whereas the residual part of the system is simulated at the MM level.[20,54,56,57] All the QM/MM calculations were performed by means of Amber12.[44,45]

During the preliminary QM/MM simulations, the QM region of the system was formed by Avi, residues Ser70, Glu166, and a water molecule, namely, Wat-R, closely interacting with both amino acids. The QM zone was simulated using the PM3-PDDG[58] Hamiltonian that, as reported by Pierdominici-Sottile and Roitberg,[59] permitted estimation of the protonation energy in *Trypanosoma cruzi trans*-sialidase with a difference below 0.5 kcal/mol with respect to the value obtained using the computationally more expensive MP2 level of theory, while the MM part of the system was simulated using the same parameters employed during the MM-MD simulations (see previous section).

The choice of this Hamiltonian is thus justified by the quality of previous benchmarks and is expected to allow the extension of a study like the present one to small-medium size libraries of designed inhibitors, which represents one of the possible evolutions of our endeavor.

The link atom approach implemented in Amber12[44,45] was employed to obtain the correct theoretical description of the bonds crossing the boundaries between QM and MM portions. The last frame of the MM-MD was used as a starting point of the QM/MM MD simulations.

The system was equilibrated for 10 ps considering the new potential. This simulation was carried on with a time step of 0.05 fs in a NVT ensemble. The temperature was set to 300 K using a Langevin thermostat with a collision frequency of 5.0 ps^{-1}.[60] Short and long-range electrostatic interactions were estimated in the same manner of classical MD.[45,51]

The activation free energy of the different steps necessary for the formation of the Avi/TEM-1 covalent complex was estimated using MTD,[28] an enhanced sampling methodology that similarly to other computational methods such as the local elevation (LE) technique,[29] conformational flooding,[61] and the Monte Carlo method of Wang and Landau accelerates rare events using history-dependent biasing potentials.[62] In this work, Gaussian shape repulsive potentials are deposed in the space described by one or more collective variables (CVs) to disfavor the system from revisiting the same region of the CVs space. The MTD method not only enables observation of rare events in an accessible, reduced (with respect to the real time scale) simulation time, but it also allows researchers to obtain the free energy surface associated with the investigated phenomenon as the negative of the deposed bias. In this work, different MTD simulation runs using different CVs were employed to define the model reaction path with the minimum activation free energy approach. The residues forming the QM region and the CVs for the description of each reaction step were selected on the basis of the chemical properties of the substrate and of the knowledge (based on existing literature) of the possible reaction mechanisms of the enzyme (Tables 1 and 2).

Table 1. Residues Included (I) in the QM Part during MTD1, MTD2, MTD3, and MTD4

Residues	MTD1	MTD2	MTD3	MTD4
Ser70	I	I	I	I
Glu166	I	I	I	I
Wat-R	I	I	I	I
Avibactam	I	I	I	I
Lys73			I	I
Ser130		I	I	I
Lys234			I	I

dx.doi.org/10.1021/bi500589x | *Biochemistry* 2014, 53, 5174−5185

Table 2. Collective Variables Considered in the Four MTD Simulations

MTD1	
CV1=A-B	A= The distance between the hydrogen atom abstracted from Wat-R and one of the oxygen atoms of the side chain belonging to Glu166
	B= The distance between the hydrogen abstracted from Wat-R and O@Wat-R.
CV2=C-D	C= The distance between the hydroxyl hydrogen atom of Ser70 and O@Wat-R.
	D= The distance between the oxygen and the hydrogen atoms of the hydroxyl group of Ser70.
CV3	E= The distance between the nitrogen atom of Lys73 side-chain and the carbon atom of the carboxylic group of Glu166.
MTD2	
CV1	A= The distance between C7@Avi and N6@Avi
CV2=B-C	B= The distance between the hydrogen abstracted from Ser130 and N7@Avi.
	C=The distance between the hydrogen and the oxygen of the hydroxyl group of Ser130.
MTD3	
CV1=A-B	A= The distance between the hydrogen abstracted from Ser130 and N7@Avi.
	B= The distance between the hydrogen and the oxygen atoms of the hydroxyl group of Ser130.
CV2	C= The distance between the oxygen atom of the hydroxyl group of Ser130 and the nitrogen atom of Lys73 side chain.
MTD4	
CV1=A-B	A= The distance between the hydrogen atom abstracted from Glu166 and the nitrogen atom of Lys73.
	B= The distance between the hydrogen atom abstracted from Glu166 and the oxygen bound to it.

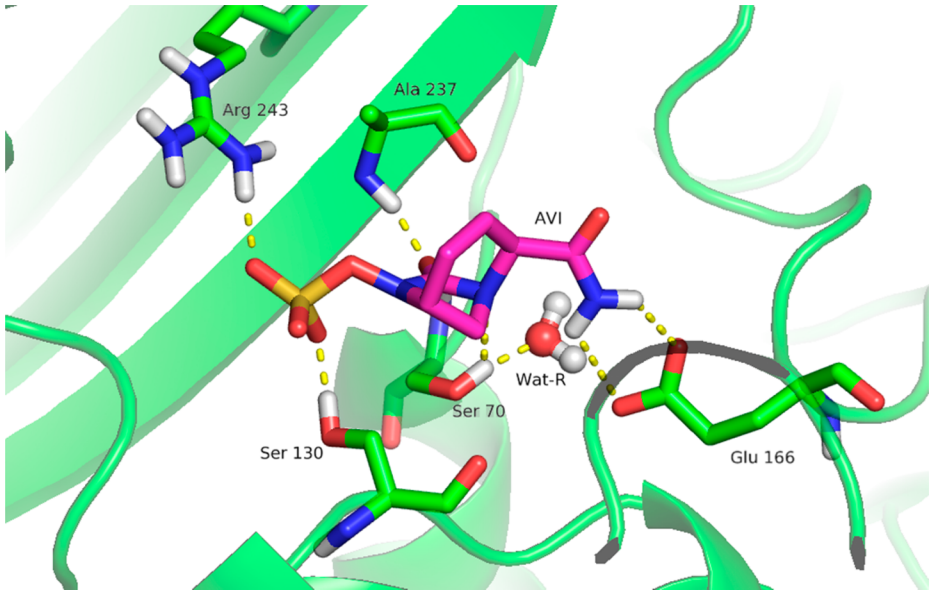

Figure 3. Representative configuration of the Avi binding geometry extracted from the last 10 ns of the MM MD simulation. For the sake of clarity, the protein is represented as ribbons, while Avi and key residues are represented as ball and stick. The main hydrogen bonds made by AVI and Wat-R are represented as dashed yellow lines.

The free energy activation barriers ($\Delta F^{\#}$) crossed during the simulations were estimated considering only the bias deposited until the phenomenon under investigation was observed, according to the methodology suggested by Laio and Gervasio[63] and in analogy with other reports.[64,65]

Especially when chemical reactivity is considered, the backward process (i.e., from product to reactants) could not to be well described by the same set of CVs used for accelerating the reactants to product transition.[66] Then, considering their computational costs, QM/MM MTD calculations are frequently stopped when the forward transition or one recrossing event was observed.[64,67,68] In this case, the $\Delta F^{\#}$ values reported for the single reaction steps are the average of the values obtained from three independent simulation runs. The statistical uncertainty was expressed as the standard deviation of the three values resulting from the independent simulations.

During MTD simulations, in order to limit the computational costs of the calculations, the space of the CVs to be explored was limited using harmonic constraints.

In all our simulations, we added repulsive Gaussian potential with a height of 0.50 kcal/mol and a width of 0.1 Å every 40 MD steps (20 fs). During our computational studies, we used MTD in its multiple walker version, to improve the computational efficiency of the computation.[69] Practically, more replicas of the system are simulated considering the same CVs and computational setup; then, at a predefined time interval, the replicas exchange information about the deposed bias, significantly reducing the time necessary to explore the free energy surface (FES). This computational scheme allows the use of more processors also in the case of the serial code of QM/MM implemented in Amber12.[44,45] In our calculations, we considered 12 replicas of the system, and the MTD simulations were extended until all the investigated steps were completed in one or more replicas.

In the multiple walkers approach, the number of replicas affects the hills deposition rate. In particular, if the single replicas are characterized by a slow diffusivity, hills could be deposited in similar places of the FES, practically increasing the rate of deposition.

In this case, we verified that the replicas rapidly evolved to different positions in the CV space, then ensuring a correct exploration of the FES. Finally, we also performed test calculations increasing/decreasing the number of replicas

dx.doi.org/10.1021/bi500589x | *Biochemistry* 2014, 53, 5174−5185

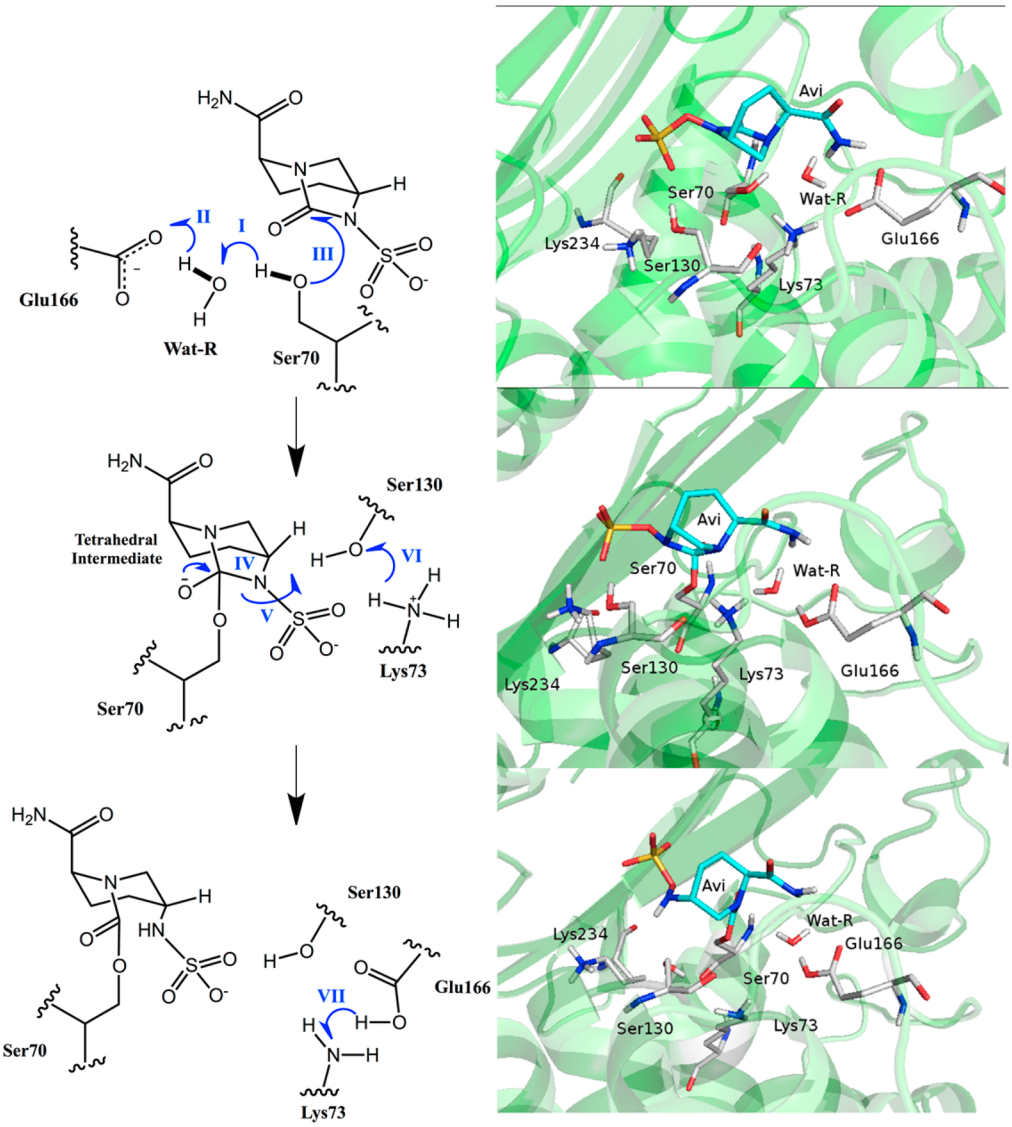

Figure 4. Graphical representation of the reaction path explored by QM/MM MTD simulations; the reaction steps are progressively numbered using roman numbers written in blue bold character. In the right column 3D structures (obtained by our simulations) corresponding to the steps displayed in the scheme. Nonpolar hydrogen atoms are not reported for clarity.

without any significant difference in the estimation of the activation barriers (not shown).

RESULTS AND DISCUSSION

MD Simulation of the TEM-1/Avibactam Complex. Structural investigation of the preliminary 70 ns long classical MD simulations of TEM-1 and of the TEM-1/Avi complex did not highlight any major macroscopic changes or distortions of the active site geometries and of the global secondary structures. The RMSD for the backbone atoms of TEM-1, calculated with respect to the starting structure during the entire simulation, was 0.91 ± 0.08 Å (Figure S1). Avi remained firmly placed in the catalytic site for the entire simulation time, conserving the same orientation and interactions observed in the starting complex. In particular, the binding of Avi within TEM-1 was reinforced by two H-bonds, the first one between the sulfate group and the side chain of Ser130 (occupancy 60%, average distance 2.7 ± 0.12 Å, average angle 14.28 ± 8.21°) and the second one between the O8@Avi and the NH group of Ala237 (occupancy 100%, average distance 2.9 ± 0.11 Å, average angle 18.65 ± 9.29°). Moreover, the oxygen atom of the side chain of Ser70 conserved a proper position to carry out the nucleophilic attack on C7@Avi with an average distance of 3.15 ± 0.16 Å (Figure 3).

A water molecule (from now on indicated as Wat-R; see also Figures 3 and 4) conserved its starting position in the catalytic site for the entire simulation time, forming stable H-bonds with residues Glu166 (occupancy 100%, average distance 2.7 ± 0.11 Å, average angle 17.60 ± 9.10°) and Ser70 (occupancy 92%, average distance 2.80 ± 0.14 Å, average angle 31.60 ± 12.95°).

Modeling of Reaction Steps. To investigate the reaction mechanism leading to the formation of the Avi-TEM complex, we hypothesized that the first acylation step involves Avi, Ser70, Glu166, and Wat-R, while residues Lys48, Ser130, and Ser234 are involved in the reaction steps subsequent to the first. This choice was initially determined by both analysis of the Avi interaction during the 70 ns long MM MD simulation and by the proposal of Blanchard and co-workers[10] for Avi inhibition in a *Mycobacterium tuberculosis* BL.

The overall reaction mechanism is reported in Figure 4. Initially, the proton of Ser70 is transferred to Glu166, shuttled by

dx.doi.org/10.1021/bi500589x | *Biochemistry* 2014, 53, 5174−5185

a water molecule (Wat-R, steps **I** and **II**, Figure 4). The resulting serinate anion attacks the β-lactam carbonyl group of Avi leading to the tetrahedral intermediate (TI, step **III**). Then, the β-lactam ring opening occurs (step **IV**), and the N6 atom of Avi is protonated by Lys73, through Ser130 (steps **V** and **VI**). Finally, Glu166 transfers its acid hydrogen to Lys73, restoring the starting protonation state of the complex (step **VII**).

Importantly, while this work was ongoing, this mechanism was further supported and confirmed by the X-ray structure solved by Lahiri et al.[11]

QM/MM MTD Calculations. Reaction Path Identification. The study of the reaction mechanism by which Avi covalently inhibits TEM-1 was carried out using MTD simulations with a QM/MM potential. Notably during these simulations, the QM part of the system was described using the PM3-PDDG[58] Hamiltonian, for which good performances in describing biocatalytic reactions were reported (see also Material and Methods).[59]

In particular, the formation of the complex was investigated splitting up the reaction steps (form **I** to **VII**, Figure 4) in four separate MTD calculations. The free energy barriers for the steps from **I** to **III** were calculated in metadynamics simulation 1 (labeled MTD1), from **IV** to **V** in MTD2, from **V** to **VI** in MTD3, and **VII** in MTD4 (Figure 5).

Preliminary studies considering a number of alternative mechanisms were carried out. However, only those addressed here were found consistent with structures available in the PDB[11] and the kinetic data.[12]

As stated in the Methods section, and reported for previous applications,[31,32] MTD requires the definition of relevant collective variables to estimate the free energy differences. Figure 5 pictorially defines the collective variables that are expected to recapitulate the relevant chemical steps of the reaction under exam, while Table 2 describes the types and definitions of CVs.

Wat-R Assists the Ser70 Deprotonation by Glu166, Steps I and II. MTD1 started from a region of the FES in which two isoenergetic minima, corresponding to the flipping of the Glu166 side chain, were identified (Figure 6). In agreement with previously reported computational[36,70] and experimental studies,[11] the water molecule (Wat-R) acts as a proton shuttle in the deprotonation of Ser70 by Glu166 (**I**–**II**). The resulting serinate makes a nucleophilic attack (**III**) on C7@Avi.

In theory the first two steps, **I**–**II**, could be properly described using only two CVs (CV1–CV2).

Previously reported computational studies by Herman et al.[36,70] as well as visual inspection of equilibration QM/MM MD simulation suggested that Lys73 could play an important role in regulating the acidity/basicity of both Ser70 and Glu166. For this reason, during MTD1, the distance between CD@Glu166 and NZ@Lys73 was considered as a collective variable (CV3). Notably, during all the replicated MTD calculations, CV3 freely oscillated between 2.5 and 5.5 Å. This behavior should guarantee that all the basins in the free energy space were filled and that the free energy space was well explored with respect to CV3. Thus, the acquired free energy surface (FES) can be confidently employed for qualitative considerations.

In depth analysis of the free energy surface (Figures 6 and S2) substantially confirmed the importance of Lys73 in Ser70 deprotonation. Indeed, we observed an increase of the CD@Glu166-NZ@Lys73 distance, together with a concomitant shortening of the OG@Ser70-NZ@Lys73 distance in all of the

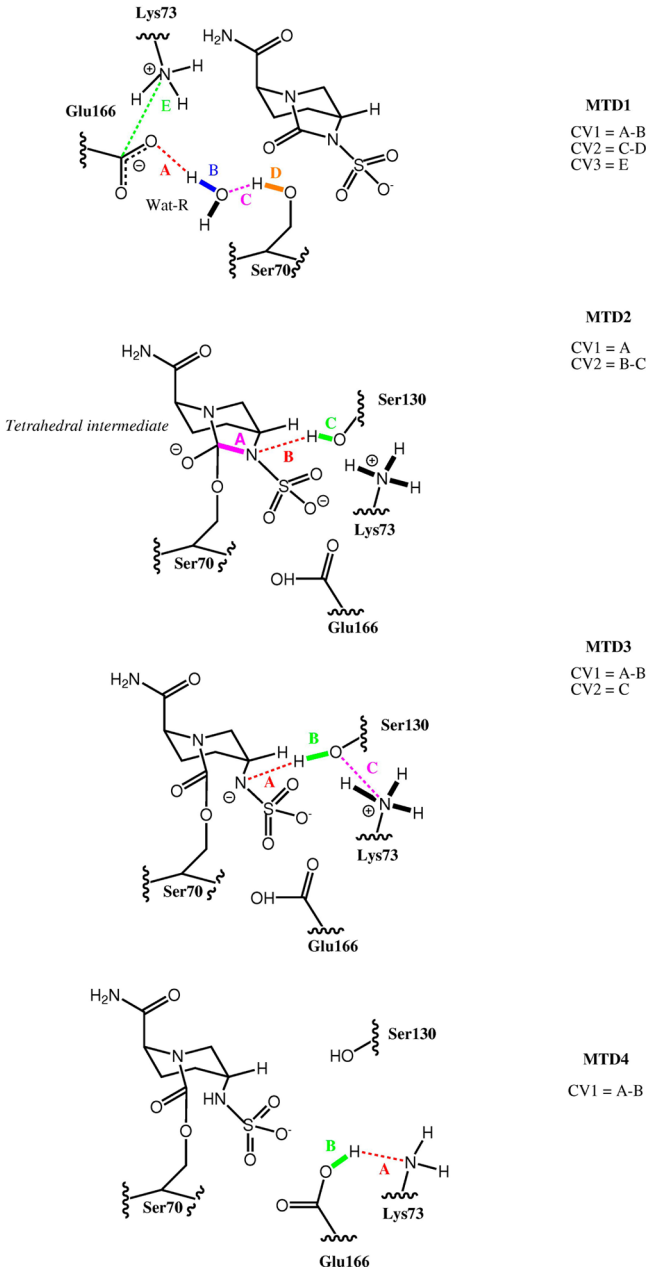

Figure 5. Graphical representation of the CVs used during the four MTD simulations carried out in this work; the bonds involved in the CV are colored as the corresponding letters.

replicated MTD simulations in which Ser70 deprotonation was monitored.

Going into further detail, the optimal CV3 value for the Ser70 deprotonation process turned out to be between 3 and 4 Å, whereas in the X-ray structure (PDB code: 1JWP) the same distance was 2.8 Å.

Simulation MTD1 also permitted a complete energetic evaluation of Ser70 deprotonation by Glu166. In the first step, a proton was first transferred from Ser70 to Glu166 (**I**) via a bridging water molecule (Wat-R), overcoming an estimated activation free energy barrier ($\Delta F^{\#}$) of 19.3 ± 0.3 kcal/mol (Figure 6A,B). In the subsequent step (**II**), Ser70 was deprotonated by the hydroxide ion derived from Wat-R with a significantly lower barrier of almost 5–6 kcal/mol (Figure 6C).

dx.doi.org/10.1021/bi500589x | *Biochemistry* 2014, 53, 5174–5185

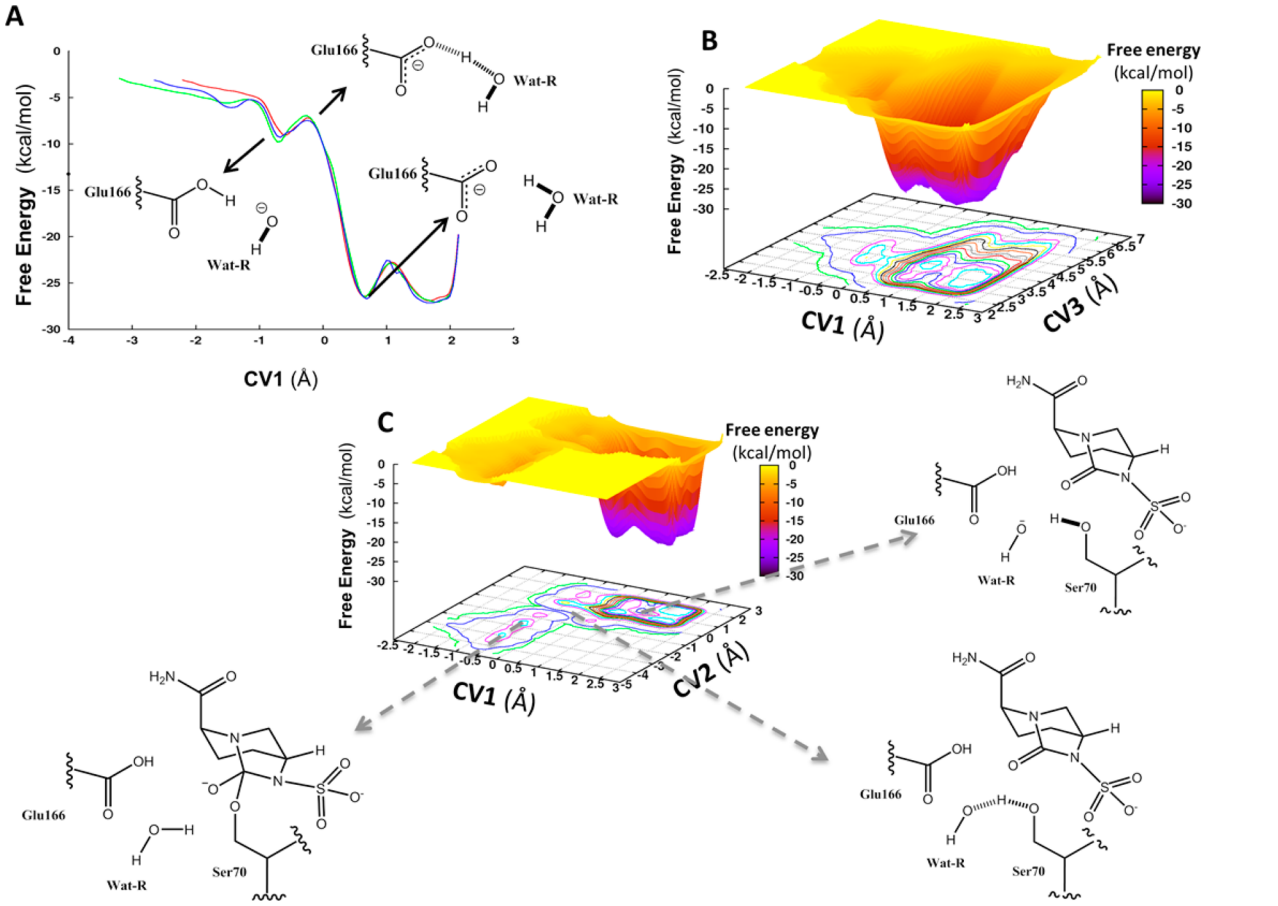

Figure 6. (A) Free energy plotted for CV1 during the three independent (line blue, red, and green) MTD1 simulations. (B, C) Free energy surfaces plotted as for CV1 vs CV3 (B) and CV1 vs CV2 (C) from one of the replicated MTD1 simulations.

It should be noticed in passing that in the one-dimensional plot of CV1 in Figure 6A, CV1 values lower than −1A are incidentally sampled. However, since we stopped the simulations once the deprotonation was observed, such regions of CV1 were not sampled enough to give a significant estimate of the free energy and the associate geometries of the complex.

Summarizing, the emerging picture for this first part of the reaction model is a water-mediated deprotonation by Glu166 in which Lys73 acts as a switch regulating acidity/basicity of the two residues involved (Ser70 and Glu166).

Ser70 Nucleophilic Attack to Avibactam and Ring Opening. During MTD1, no CVs (Figure 5) were explicitly considered for describing the nucleophile attack of Ser70 to C7@Avi (**III**) and the formation of the tetrahedral intermediate (**TI**). The nucleophilic attack of Ser70 took place in coordination to the evolution of the system along the chosen relevant CVs, which do not include a bias involving Ser70. In this respect, it can be considered as a spontaneous nucleophilic attack. Literature described the **TI** (Figures 4 and 6) as a relatively stable chemical entity.[17,71] Nevertheless, Tripathi and Nair[33] recently postulated a spontaneous four-member ring aperture, estimating $\Delta F^{\#}$ values of 2−4 kcal/mol for cephalotin and aztreonam.

Therefore, in order to test the stability of our **TI** in a reasonable time interval, we performed a 40 ps QM/MM MD simulation (in this simulation the same computational setup of MTD1 was used). The obtained trajectory showed that the spontaneous ring opening did not occur, and the geometry of the **TI** was stable during the whole simulation time. Moreover, we observed that Wat-R mainly conserved its position forming a stable H-bond interaction with Glu166, while Lys73 formed analogous interactions with the side chain oxygen of Ser70 and the backbone carbonyl group of Ser130.

For this reason, we performed MTD2 calculations in which the C7−N6@Avi bond breakage (**IV**) and the proton transfer from Ser130 to N6@Avi (**V**) were explored. The choice to consider Ser130 as a putative hydrogen donor emerged from both visual inspection of our simulation trajectories and structural studies reported by Docquier and co-workers.[11]

In all the replicated MTD2 simulations, started from the **TI** (α in Figure 7A), we first observed the reaction evolution to a free energy minimum in which the C7−N6@Avi bond was completely broken (β in Figure 7A), overcoming a $\Delta F^{\#}$ of 18.1 ± 0.6 kcal/mol. It is to be stated that in this case no recrossing event was observed, and the average value plus standard deviations were calculated on the basis of 3 simulations as stated in Materials and Methods. Next, the proton transfer between Ser130 to N6@Avi took place overcoming an estimated $\Delta F^{\#}$ of ∼21 ± 5 kcal/mol (γ in Figure 7B).

It is important to underline that a high measured standard deviation, such as the one observed for the formation of γ, is usually due to rare events not properly taken into account during MTD simulations. Thus, we evaluated the possibility to consider different/additional CVs in supplementary MTD calculations (MTD3).

N6@Avi Protonation and Final Adduct Formation. Docquier and co-workers[11] suggested that in Avi/CTX-M-15 and Avi/AmpC complexes, residue Lys73 facilitates the deprotonation process of Ser130. Consequently, we carried out

dx.doi.org/10.1021/bi500589x | Biochemistry 2014, 53, 5174−5185

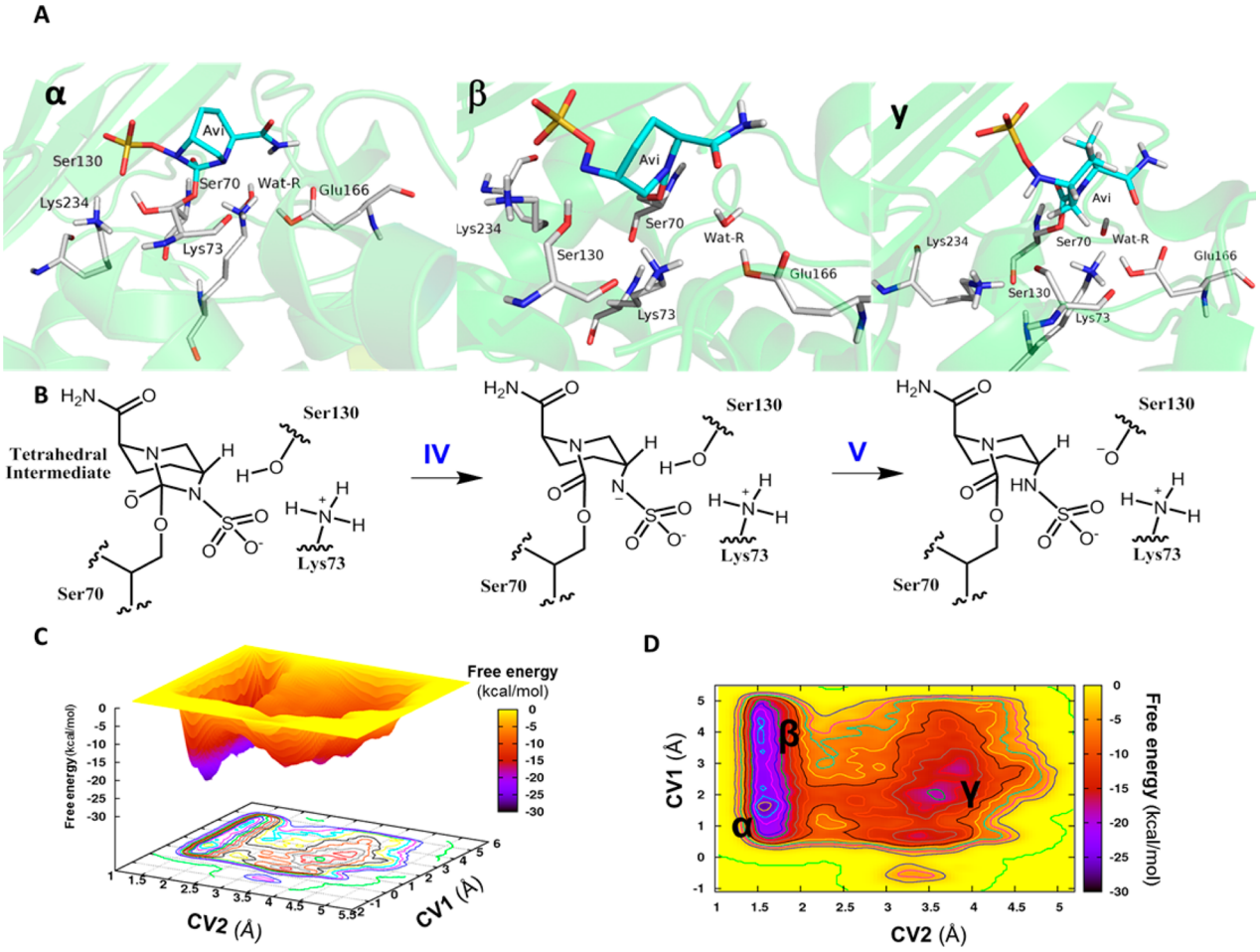

Figure 7. (A) Representative structures of the catalytic site in the three minima (α, β, and γ) visited during MTD2. (B) Corresponding 2-D scheme, (C–D) different views of the same FES derived from one of the replicated MTD2 simulation. Nonpolar hydrogen atoms are not reported for clarity.

MTD simulations (MTD3) in which Lys73 was included in the QM part of the system, together with Lys234 similarly adjacent to Ser130. For the same reason, in MTD3 we considered as CV the distance between NZ@Lys73 and OG@Ser130 (CV2, Figure 5 and Table 2). The calculations started from a conformation of the complex in which the C7–N6@Avi bond was already broken, thus only the activation free energy for the proton transfer from OG@Ser130 to N6@Avi (**V**) was estimated.

From the calculations, CV2 emerged as necessary for the optimal description of the reaction step under investigation. Specifically, the proton transfer occurred overcoming a $\Delta F^{\#}$ of 13.2 ± 0.9 kcal/mol when the CV2 value was between 2.5 and 2.8 Å, the ideal distance needed to generate a H-bond between two heavy atoms (Figure 8). Notably, in this set of simulations, by means of three CVs a better description of the processes under investigation was obtained and a lower $\Delta F^{\#}$ value was estimated, 21 ± 5 kcal/mol by MTD2 vs 13.2 ± 0.9 kcal/mol by MTD3.

Strikingly, Lys73 spontaneously transferred one of its proton to the Ser130 anion form (**VI**), indicating that this step is barrierless, and it is very likely to be concerted with the previous reaction step. Therefore, at the end of MTD3, Avi, Lys73 and Glu166 assumed their neutral forms (Figure 8).

Also in this case it is worth noting that Lys73-Ser130 proton transfer is not explicitly considered in the CVs, and it happens as a function of the sampling along the other relevant CVs.

In brief, the outputs from MTD2 and MTD3 support a reaction model in which, starting from a stable TI, the breakage of the C7–N6@Avi bond is first observed with a $\Delta F^{\#}$ of 18.1 ± 0.6 kcal/mol, and then a proton is transferred to N6@Avi by Lys73 through Ser130 overcoming a barrier of 13.2 ± 0.9 kcal/mol.

Proton Transfer from Glu166 to Lys73. Finally, to investigate mechanisms taking the protein back to its original protonation state, the proton transfer from Glu166 to Lys73 (**VII**) was evaluated. To this aim, in MTD4 (Figure 5) the main CV was defined as the difference of (i) the distance between the proton bound to Glu166 and NZ@Lys73, and (ii) the distance between that hydrogen atom and OE@Glu166. With these parameters, MTD4 we estimated a $\Delta F^{\#}$ value of 29.5 ± 3.2 kcal/mol (Figure 9).

For the same reaction step, Hermann et al.[70] reported a problematic estimation of the activation barrier, when both DFT and semiempirical methods were applied. However, in our case, considering the similarity of the estimation over all the replicated simulations, the average $\Delta F^{\#}$ value is sufficiently accurate to be utilized at least for qualitative considerations.

Recent studies[13] indicated that the Avi inhibition profile is compatible with a reversible covalent inhibition. In this respect, on the basis of our model and estimates, due to the high barrier of the last investigated step, the inhibition process involving Avi was complete when its five-membered ring was cleaved and Glu166/Lys73 were in their neutral form. In this framework, Lahiri et al.[11]

dx.doi.org/10.1021/bi500589x | *Biochemistry* 2014, 53, 5174–5185

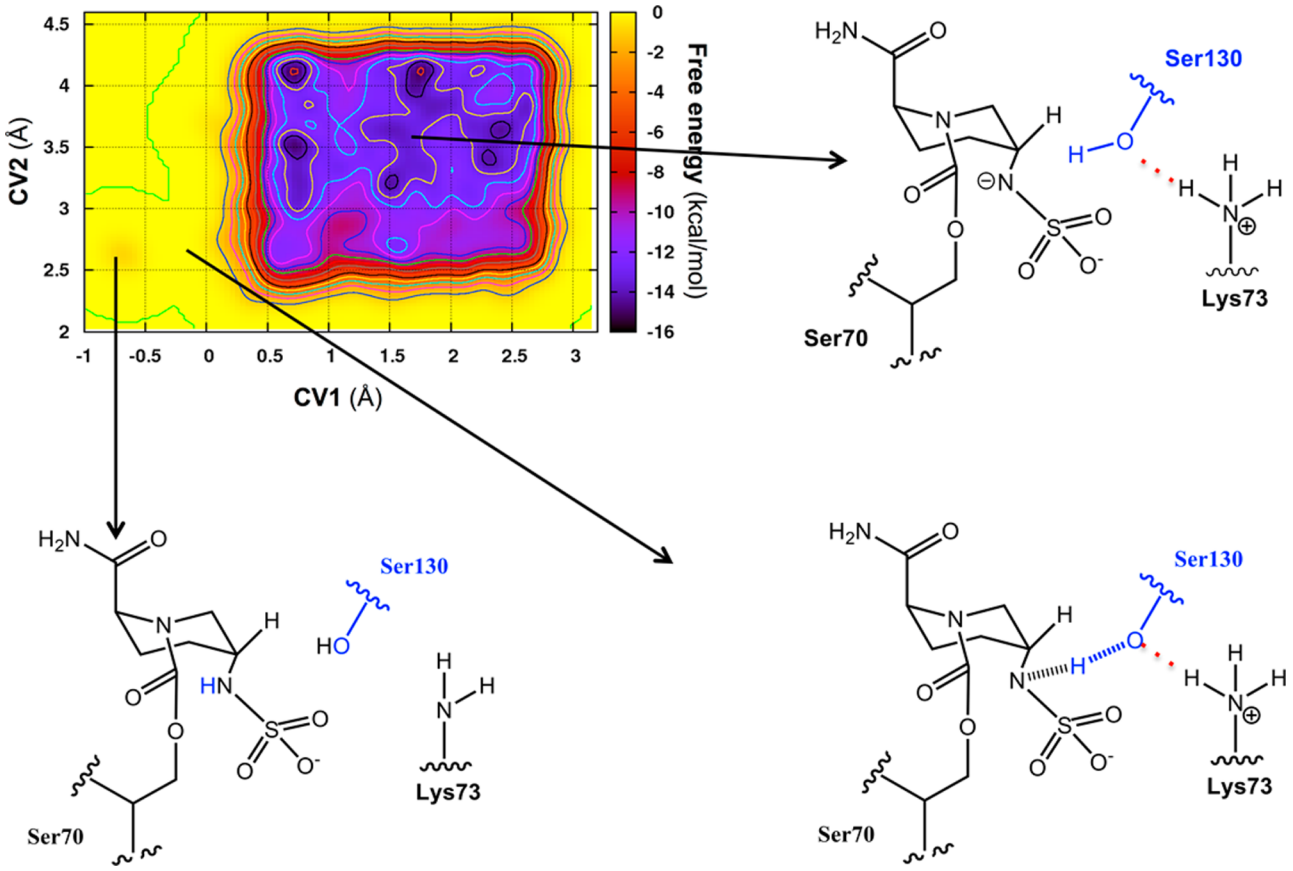

Figure 8. Free energy surface as a function of CV1 and CV2 after proton transfer from Ser130 to N6@Avi. FES derived from MTD3 simulation.

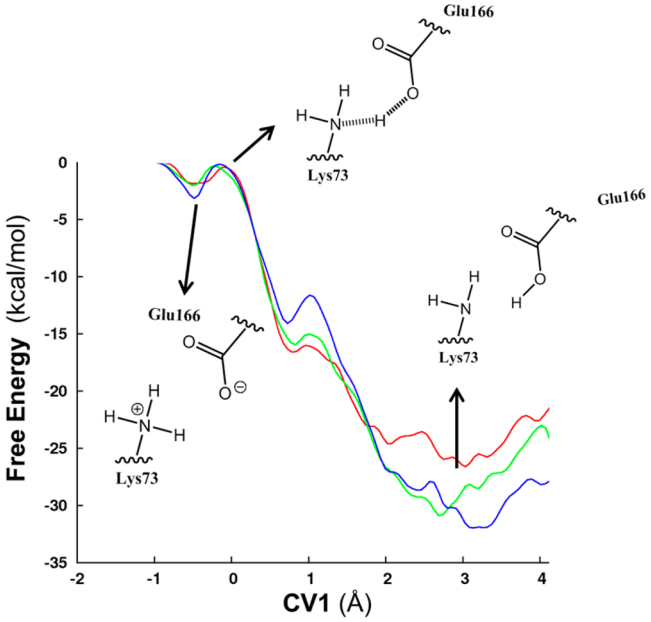

Figure 9. Free energy profile as a function of CV1 during the three replicated MTD4 simulations.

suggested that the anionic form of Glu166, able to activate a water molecule coming from the bulk, could be required for the hydrolytic release of Avi. The high $\Delta F^{\#}$ value estimated for the proton transfer from Glu166 and Lys73 could help explain the reason why the deacylation ring-closure event is favored over the hydrolytic release of the inhibitor. However, investigating Avi reversibility is beyond the goal of this study, and additional computational investigations would be necessary to clarify this and other aspects of the inhibition process.

CONCLUSIONS

This study has been primarily aimed at contributing to clarify the mechanism and the energetic aspects of formation of the complex between TEM-1 BL and the novel generation inhibitor avibactam. We approached this problem using classical MD simulations and metadynamics based QM/MM calculations to model the systems representing the different stages involved in the formation of a covalent bond between avibactam and TEM-1. Through this approach, we reproduced activation energy values for the formation of relevant intermediates, which are in good agreement with experimentally determined parameters. In particular, we were able to identify the minimal activation free energies ($\Delta F^{\#}$) reaction pathway.

The estimated values were in line with previously reported kinetic data,[12] and the favored mechanism was compatible with structural data.[11] The formation of the avibactam/TEM-1 covalent complex started with the deprotonation of a catalitycally active water (Wat-R) by Glu166 (**I**, $\Delta F^{\#}$ 19.3 ± 0.3 kcal/mol), followed by Ser70 deprotonation (**II**) with a lower $\Delta F^{\#}$ ∼5−6 kcal/mol. Consequently, we observed the spontaneous formation of a tetrahedral intermediate (**III**) followed by the opening of the five-membered ring of avibactam (**IV**, $\Delta F^{\#}$ 18.1 ± 0.6). Then, once the five-membered ring of Avi was completely open, Ser130 transferred its proton atom to N6 (**V**) with a $\Delta F^{\#}$ value of 13.2 ± 0.9 kcal/mol, and next the neutral form of Ser130 was restored by a spontaneous proton transfer from Lys73 (**VI**).

dx.doi.org/10.1021/bi500589x | *Biochemistry* 2014, 53, 5174−5185

Finally, the deprotonated form of Glu166 was regenerated via a proton transfer from Glu166 to NZ@Lys73 (**VII**, $\Delta F^{\#} = 29.5 \pm 3.2$ kcal/mol).

On the basis of these computational results and their comparisons with experimental evaluations, combined with the consideration that the rate-determining step (having the highest activation free energy barrier) determines the overall rate of a complex reaction mechanism, we hypothesize that the water-assisted Glu166 deprotonation by Ser70 represents the limiting step for the enzymatic reaction under investigation. For this step, we estimated a $\Delta F^{\#}$ value of 19.3 ± 0.3 kcal/mol, while the corresponding expected value calculated applying the Eyring equation on the experimental kinetic data was 18.8 kcal/mol.[12]

Additionally, our simulations confirmed the essential role played by Lys73 in lowering the free energy barrier that have to be overcome to favor the Ser70 and Ser130 deprotonation precesses.

When our study was in an advanced phase, two structures of Avi in complex with a class A and a class C BL were solved and made available in the PDB.[11] Interestingly, our findings are substantially supported and corroborate the mechansistic hypotheses derived from these structural data.

As an important caveat, it has to be noted that our results represent only a semiquantitative evaluation of the reaction energetics: indeed, our aim is to provide an estimate of the activation energy barriers and, in this context, we are neither considering the full sampling of the product state nor consequently recrossing events taking the system back from the products to the reactants. Statistics and error bars are obtained here through multiple simulations. However, the use of this relatively simple, but computationally less expensive, level of theory enabled us to accomplish a reasonably exhaustive sampling of the conformational space of the systems on one hand and to evaluate different reaction pathways on the other.

Importantly, the use of a simplified and computationally tractable Hamiltonian, whose performance has been carefully benchmarked here and in previous papers by others,[59,72] holds promise for future applications in the study of different analogues of avibactam, opening up the possibility to include explicit mechanistic calculations and enzyme−substrate dynamics correlations in the design of novel derivatives with improved profiles, in the development of new chemical entities able to target and inhibit a wider spectrum of BLs and in understanding the determinants of different inhibition profiles across BLs.

Specifically, our approach can represent a viable method for obtaining atomic-resolution insights into the principal mechanism of action of a novel generation, highly promising antibiotic, whose novel structure and mode of action could be key to solving problems related to the development of drug resistance in Gram-negative bacteria. The information on the inhibitor−enzyme cross-talk, and modulation of the active site structural dynamics, can in fact be exploited to define the positions where the addition/variation of specific chemical functionalities on the existing scaffold allows for the optimization of the interactions with a specific stereochemical and electrostatic environments (that would not be accessible in single-structure models or classical MD simulations), as well as for the extensions of binding interactions into previously uncharacterized regions or pockets.

Indeed, the formation/disappearance of pockets due to the conformational response of the protein to the first-generation inhibitor can be used to define the stereochemical properties of functional groups that need to be linked to the scaffolds, to facilitate optimal fitting to the variations in the shape and properties of the active site. In perspective, the concepts and methods developed in this paper could be used to carry out extensive comparative studies considering the X-ray structures of Avi/class A and a class C BL complexes.[11] Complementarily, one may envisage studying the inhibition of more than one member of BLs, as Avi may bind to any BLs and not only to that studied here.

These two latter points clearly represent goals that are well beyond the scope of this first study, and they would require a computational effort, which would still be massive even for today's standards. However, we are confident that the steady improvement in software and hardware performance will facilitate obtaining these ambitious goals in the near future.

In conclusion, we envisage that our approach together with the protocols herein adopted may represent a relevant example of the application of QM/MM free energy calculations to the study of complex biochemical reactions, which in principle could be a valuable tool in the broader context of drug discovery and development.

■ ASSOCIATED CONTENT

Supporting Information

RMSD over the 70 ns of MD simulation (Figure S1) and the 3D and 2D plots of the FESs obtained by MTD1 (Figure S2). This material is available free of charge via the Internet at http://pubs.acs.org.

■ AUTHOR INFORMATION

Corresponding Author

*Tel.: +39 02 285 000 31. Fax: +39 02 289 012 39. E-mail: giorgio.colombo@icrm.cnr.it.

Author Contributions

#J.S. and G.G. equally contributed to this work.

Funding

This work was supported by CARIPLO "From Genome to Antigen: A Multidisciplinary Approach towards the Development of an Effective Vaccine against *Burkholderia pseudomallei*, the Etiological Agent of Melioidosis" (Contract Number 2009-3577). Support was also received from AIRC (Associazione Italiana Ricerca sul Cancro), Grant IG.11775 to G.C., and by the Italian Ministry of Education and Research through the Flagship (PB05) "InterOmics". We acknowledge CINECA and the Regione Lombardia award under the LISA initiative, for the availability of high performance computing resources and support.

Notes

The authors declare no competing financial interest.

■ ACKNOWLEDGMENTS

We acknowledge Dr. Davide Branduardi for implementation of the charge rescaling approach.

■ REFERENCES

(1) Drawz, S. M., and Bonomo, R. A. (2010) Three decades of beta-lactamase inhibitors. *Clin. Microbiol. Rev. 23*, 160−201.

(2) Perez-Llarena, F. J., and Bou, G. (2009) Beta-lactamase inhibitors: the story so far. *Curr. Med. Chem. 16*, 3740−3765.

(3) Chen, J., Shang, X., Hu, F., Lao, X., Gao, X., Zheng, H., and Yao, W. (2013) β-Lactamase Inhibitors: An Update. *Mini Rev. Med. Chem. 13*, 1846−1861.

(4) Bush, K., and Jacoby, G. A. (2010) Updated functional classification of beta-lactamases. *Antimicrob. Agents Chemother. 54*, 969−976.

(5) Crowder, M. W., Spencer, J., and Vila, A. J. (2006) Metallo-beta-lactamases: novel weaponry for antibiotic resistance in bacteria. *Acc. Chem. Res. 39*, 721−728.
(6) Bebrone, C., Lassaux, P., Vercheval, L., Sohier, J.-S., Jehaes, A., Sauvage, E., and Galleni, M. (2010) Current challenges in antimicrobial chemotherapy: focus on β-lactamase inhibition. *Drugs 70*, 651−679.
(7) Farina, D., Spyrakis, F., Venturelli, A., Cross, S., Tondi, D., and Costi, M. P. (2014) The inhibition of extended spectrum β -lactamases: hits and leads. *Curr. Med. Chem. 21*, 1405−1434.
(8) Shlaes, D. M. (2013) New β-lactam−β-lactamase inhibitor combinations in clinical development. *Ann. N.Y. Acad. Sci. 1277*, 105−114.
(9) Ehmann, D. E., Jahic, H., Ross, P. L., Gu, R. F., Hu, J., Durand-Reville, T. F., Lahiri, S., Thresher, J., Livchak, S., Gao, N., Palmer, T., Walkup, G. K., and Fisher, S. L. (2013) Kinetics of avibactam inhibition against class A, C, and D β-lactamases. *J. Biol. Chem. 288*, 27960−27971.
(10) Xu, H., Hazra, S., and Blanchard, J. S. (2012) NXL104 Irreversibly Inhibits the β-Lactamase from Mycobacterium tuberculosis. *Biochemistry 51*, 4551−4557.
(11) Lahiri, S. D., Mangani, S., Durand-Reville, T., Benvenuti, M., De Luca, F., Sanyal, G., and Docquier, J. D. (2013) Structural Insight into Potent Broad-spectrum Inhibition with Reversible Recyclization Mechanism: Avibactam in Complex with CTX-M-15 and Pseudomonas aeruginosa AmpC β-lactamases. *Antimicrob. Agents Chemother. 57*, 2496−2505.
(12) Stachyra, T., Pechereau, M. C., Bruneau, J.-M., Claudon, M., Frere, J.-M., Miossec, C., Coleman, K., and Black, M. T. (2010) Mechanistic studies of the inactivation of TEM-1 and P99 by NXL104, a novel non-beta-lactam beta-lactamase inhibitor. *Antimicrob. Agents Chemother. 54*, 5132−5138.
(13) Ehmann, D. E., Jahi, H., Ross, P. L., Gu, R.-F., Hu, J., Kern, G., Walkup, G. K., and Fisher, S. L. (2012) Avibactam is a covalent, reversible, non-β-lactam β-lactamase inhibitor. *Proc. Natl. Acad. Sci. U.S.A. 109*, 11663−11668.
(14) Wang, X., Minasov, G., and Shoichet, B. K. (2002) Evolution of an antibiotic resistance enzyme constrained by stability and activity trade-offs. *J. Mol. Biol. 320*, 85−95.
(15) DÌaz, N., Suarez, D., Merz, K. M., and Sordo, T. s. L. (2005) Molecular dynamics simulations of the TEM-1 beta-lactamase complexed with cephalothin. *J. Med. Chem. 48*, 780−791.
(16) Pimenta, A. C., Martins, J. M., Fernandes, R., and Moreira, I. S. (2013) Ligand-Induced Structural Changes in TEM-1 Probed by Molecular Dynamics and Relative Binding Free Energy Calculations. *J. Chem. Inf. Model. 53*, 2648−2658.
(17) Meroueh, S. O., Fisher, J. F., Schlegel, H. B., and Mobashery, S. (2005) Ab initio QM/MM study of class A beta-lactamase acylation: dual participation of Glu166 and Lys73 in a concerted base promotion of Ser70. *J. Am. Chem. Soc. 127*, 15397−15407.
(18) Tozzini, V. (2009) Multiscale modeling of proteins. *Acc. Chem. Res. 43*, 220−230.
(19) Sgrignani, J., and Magistrato, A. (2013) First-Principles Modeling of Biological Systems and Structure-Based Drug-Design. *Curr. Comput.-Aided. Drug. Des. 9*, 15−34.
(20) Warshel, A., and Levitt, M. (1976) Theoretical studies of enzymic reactions: dielectric, electrostatic and steric stabilization of the carbonium ion in the reaction of lysozyme. *J. Mol. Biol. 103*, 227−249.
(21) De Vivo, M. (2011) Bridging quantum mechanics and structure-based drug design. *Front. Biosci. 16*, 1619−1633.
(22) Náray-Szabó, G., Oláh, J., and Krámos, B. z. (2013) Quantum Mechanical Modeling: A Tool for the Understanding of Enzyme Reactions. *Biomolecules 3*, 662−702.
(23) Colombo, G., and Carrea, G. (2002) Modeling enzyme reactivity in organic solvents and water through computer simulations. *J. Biotechnol. 96*, 23−33.
(24) Spiegel, K., and Magistrato, A. (2006) Modeling anticancer drug-DNA interactions via mixed QM/MM molecular dynamics simulations. *Org. Biomol. Chem. 4*, 2507−2517.
(25) Cavalli, A., Carloni, P., and Recanatini, M. (2006) Target-related applications of first principles quantum chemical methods in drug design. *Chem. Rev. 106*, 3497−3519.
(26) Lodola, A., and De Vivo, M. (2012) The increasing role of QM/MM in drug discovery. *Adv. Protein Chem. Struct. Biol. 87*, 337−362.
(27) Lodola, A., and Mulholland, A. J. (2013) Computational enzymology. *Methods Mol. Biol. 924*, 67−89.
(28) Laio, A., and Parrinello, M. (2002) Escaping free-energy minima. *Proc. Natl. Acad. Sci. U. S. A. 99*, 12562−12566.
(29) Huber, T., Torda, A. E., and van Gunsteren, W. F. (1994) Local elevation: a method for improving the searching properties of molecular dynamics simulation. *J. Comput.-Aided Mol. Des. 8*, 695−708.
(30) Abrams, C., and Bussi, G. (2013) Enhanced Sampling in Molecular Dynamics Using Metadynamics, Replica-Exchange, and Temperature-Acceleration. *Entropy 16*, 163−199.
(31) Barducci, A., Bonomi, M., and Parrinello, M. (2011) *Metadynamics, Wiley Interdisciplinary Reviews: Computational Molecular Science. 1*, 826−843.
(32) Ensing, B., De Vivo, M., Liu, Z., Moore, P., and Klein, M. L. (2006) Metadynamics as a tool for exploring free energy landscapes of chemical reactions. *Acc. Chem. Res. 39*, 73−81.
(33) Tripathi, R., and Nair, N. N. (2013) Mechanism of Acyl-Enzyme Complex Formation from the Henry-Michaelis Complex of Class C β-Lactamases with β-Lactam Antibiotics. *J. Am. Chem. Soc. 135*, 14679−14690.
(34) Petersen, L., ArdËvol, A., Rovira, C., and Reilly, P. J. (2010) Molecular mechanism of the glycosylation step catalyzed by Golgi alpha-mannosidase II: a QM/MM metadynamics investigation. *J. Am. Chem. Soc. 132*, 8291−8300.
(35) Anandakrishnan, R., Aguilar, B., and Onufriev, A. V. (2012) H++ 3.0: automating pK prediction and the preparation of biomolecular structures for atomistic molecular modeling and simulations. *Nucleic. Acids Res. 40*, W537−541.
(36) Hermann, J. C., Pradon, J., Harvey, J. N., and Mulholland, A. J. (2009) High Level QM/MM Modeling of the Formation of the Tetrahedral Intermediate in the Acylation of Wild Type and K73A Mutant TEM-1 Class A β-Lactamase. *J. Phys. Chem. A 113*, 11984−11994.
(37) Minasov, G., Wang, X., and Shoichet, B. K. (2002) An Ultrahigh Resolution Structure of TEM-1 β-Lactamase Suggests a Role for Glu166 as the General Base in Acylation. *J. Am. Chem. Soc. 124*, 5333−5340.
(38) Xu, H., Hazra, S., and Blanchard, J. S. (2012) NXL104 irreversibly inhibits the β-lactamase from Mycobacterium tuberculosis. *Biochemistry 51*, 4551−4557.
(39) Frisch, M. J.; G. W. T, Schlegel, H. B.; Scuseria, G. E.; Robb, M. A.; Cheeseman, J. R.; Scalmani, G.; Barone, V.; Mennucci, B.; Petersson, G. A.; Nakatsuji, H.; Caricato, M.; Li, X.; Hratchian, H. P.; Izmaylov, A. F.; Bloino, J.; Zheng, G.; Sonnenberg, J. L.; Hada, M.; Ehara, M.; Toyota, K.; Fukuda, R.; Hasegawa, J.; Ishida, M.; Nakajima, T.; Honda, Y.; Kitao, O.; Nakai, H.; Vreven, T.; Montgomery, J. A.; , Jr., Peralta, J. E.; Ogliaro, F.; Bearpark, M.; Heyd, J. J.; Brothers, E.; Kudin, K. N.; Staroverov, V. N.; Kobayashi, R.; Normand, J.; Raghavachari, K.; Rendell, A.; Burant, J. C.; Iyengar, S. S.; Tomasi, J.; Cossi, M.; Rega, N.; Millam, J. M.; Klene, M.; Knox, J. E.; Cross, J. B.; Bakken, V.; Adamo, C.; Jaramillo, J.; Gomperts, R.; Stratmann, R. E.; Yazyev, O.; Austin, A. J.; Cammi, R.; Pomelli, C.; Ochterski, J. W.; Martin, R. L.; Morokuma, K.; Zakrzewski, V. G.; Voth, G. A.; Salvador, P.; Dannenberg, J. J.; Dapprich, S.; Daniels, A. D.; Ö. Farkas, Foresman, J. B.; Ortiz, J. V.; Cioslowski, J.; , and D. J. Fox (2009) Gaussian 09, Revision A.1.
(40) Becke, A. D. (1988) Density-functional exchange-energy approximation with correct asymptotic behavior. *Phys. Rev. A 38*, 3098.
(41) Becke, A. D. (1993) Density-functional thermochemistry. III. The role of exact exchange. *J. Chem. Phys. 98*, 5648−5652.
(42) Cornell, W. D., Cieplak, P., Bayly, C. I., and Kollmann, P. A. (1993) Application of RESP charges to calculate conformational energies, hydrogen bond energies, and free energies of solvation. *J. Am. Chem. Soc. 115*, 9620−9631.

(43) Jorgensen, W. L., Chandrasekhar, J., Madura, J. D., Impey, R. W., and Klein, M. L. (1983) Comparison of simple potential funtions for simulating liquid water. *J. Chem. Phys. 79*, 926−935.
(44) Case, D. A., Darden, T. A., Cheatham, T. E., III, Simmerling, C. L., Wang, J., Duke, R. E., Luo, R., Walker, R. C., Zhang, W., Merz, K. M., Roberts, B., Hayik, S., Roitberg, A., Seabra, G., Swails, J., Goetz, A. W., Kolossváry, I., Wong, K. F., Paesani, F., Vanicek, J., Wolf, R. M., Liu, J., Wu, X., Brozell, S. R., Steinbrecher, T., Gohlke, H., Cai, Q., Ye, X., Wang, J., Hsieh, M.-J., Cui, G., Roe, D. R., Mathews, D. H., Seetin, M. G., Salomon-Ferrer, R., Sagui, C.; Babin, V., Luchko, T., Gusarov, S., Kovalenko, A., and Kollman, P. A. (2012) *AMBER12*, University of California.
(45) Walker, R. C., Crowley, M. F., and Case, D. A. (2008) The implementation of a fast and accurate QM/MM potential method in Amber. *J. Comput. Chem. 29*, 1019−1031.
(46) Wang, J., Wolf, R. M., Caldwell, J. W., Kollman, P. A., and Case, D. A. (2004) Development and testing of a general amber force field. *J. Comput. Chem. 25*, 1157−1174.
(47) Grazioso, G., Limongelli, V., Branduardi, D., Novellino, E., De Micheli, C., Cavalli, A., and Parrinello, M. (2012) Investigating the mechanism of substrate uptake and release in the glutamate transporter homologue Glt(Ph) through metadynamics simulations. *J. Am. Chem. Soc. 134*, 453−463.
(48) D'Amore, C., Di Leva, F. S., Sepe, V., Renga, B., Del Gaudio, C., D'Auria, M. V., Zampella, A., Fiorucci, S., and Limongelli, V. (2014) Design, synthesis, and biological evaluation of potent dual agonists of nuclear and membrane bile acid receptors. *J. Med. Chem. 57*, 937−954.
(49) Di Leva, F. S., Festa, C., D'Amore, C., De Marino, S., Renga, B., D'Auria, M. V., Novellino, E., Limongelli, V., Zampella, A., and Fiorucci, S. (2013) Binding mechanism of the farnesoid X receptor marine antagonist suvanine reveals a strategy to forestall drug modulation on nuclear receptors. Design, synthesis, and biological evaluation of novel ligands. *J. Med. Chem. 56*, 4701−4717.
(50) Limongelli, V., Bonomi, M., and Parrinello, M. (2013) Funnel metadynamics as accurate binding free-energy method. *Proc. Natl. Acad. Sci. U S A 110*, 6358−6363.
(51) Essmann, U., Perera, L., Berkowitz, M. L., Darden, T., Lee, H., and Pedersen, L. G. (1995) A smooth particle mesh Ewald method. *J. Chem. Phys. 103*, 8577−8593.
(52) Ryckaert, J. P., Ciccotti, G., and Berendsen, H. J. C. (1977) Numerical integration of the cartesian equations of motion of a system with constraints: molecular dynamics of n-alkanes. *J. Comput. Phys. 23*, 327−341.
(53) Humphrey, W., Dalke, A., and Schulten, K. (1996) VMD: visual molecular dynamics. *J. Mol. Graph. 14*, 33−38.
(54) Senn, H. M., and Thiel, W. (2009) QM/MM methods for biomolecular systems. *Angew. Chem., Int. Ed. Engl. 48*, 1198−1229.
(55) Otyepka, M., Banas, P., Magistrato, A., Carloni, P., and Damborsky, J. (2008) Second step of hydrolytic dehalogenation in haloalkane dehalogenase investigated by QM/MM methods. *Proteins. 70*, 707−717.
(56) Lonsdale, R., Ranaghan, K. E., and Mulholland, A. J. (2010) Computational enzymology. *Chem. Commun. 46*, 2354−2372.
(57) Dal Peraro, M., Ruggerone, P., Raugei, S., Gervasio, F. L., and Carloni, P. (2007) Investigating biological systems using first principles Car-Parrinello molecular dynamics simulations. *Curr. Opin. Struct. Biol. 17*, 149−156.
(58) Repasky, M. P., Chandrasekhar, J., and Jorgensen, W. L. (2002) PDDG/PM3 and PDDG/MNDO: improved semiempirical methods. *J. Comput. Chem. 23*, 1601−1622.
(59) Pierdominici-Sottile, G., and Roitberg, A. E. (2010) Proton Transfer Facilitated by Ligand Binding. An Energetic Analysis of the Catalytic Mechanism of Trypanosoma cruzi Trans-Sialidase. *Biochemistry. 50*, 836−842.
(60) Loncharich, R. J., Brooks, B. R., and Pastor, R. W. (1992) Langevin dynamics of peptides: the frictional dependence of isomerization rates of N-acetylalanyl-N′-methylamide. *Biopolymers 32*, 523−535.
(61) Grubmuller, H. (1995) Predicting slow structural transitions in macromolecular systems: Conformational flooding. *Phys. Rev. E 52*, 2893−2906.
(62) Wang, F., and Landau, D. P. (2001) Efficient, multiple-range random walk algorithm to calculate the density of states. *Phys. Rev. Lett. 86*, 2050−2053.
(63) Laio, A., and Gervasio, F. (2008) Metadynamics: a method to simulate rare events and reconstruct the free energy in biophysics, chemistry and material science. *Rep. Prog. Phys. 71*, 126601.
(64) Ma, C., Piccinin, S., and Fabris, S. (2012) Reaction Mechanisms of Water Splitting and H2 Evolution by a Ru(II)-Pincer Complex Identified with Ab Initio Metadynamics Simulations. *ACS Catal. 2*, 1500−1506.
(65) Bisha, I., Laio, A., Magistrato, A., Giorgetti, A., and Sgrignani, J. (2013) A Candidate Ion-Retaining State in the Inward-Facing Conformation of Sodium/Galactose Symporter: Clues from Atomistic Simulations. *J. Chem. Theory Comput. 9*, 1240−1246.
(66) Alfonso-Prieto, M., Biarnes, X., Vidossich, P., and Rovira, C. (2009) The molecular mechanism of the catalase reaction. *J. Am. Chem. Soc. 131*, 11751−11761.
(67) Cantu, D. C., Ardevol, A., Rovira, C., and Reilly, P. J. (2014) Molecular Mechanism of a Hotdog-Fold Acyl-CoA Thioesterase. *Chemistry 20*, 9045−9051.
(68) Petersen, L., Ardevol, A., Rovira, C., and Reilly, P. J. (2010) Molecular mechanism of the glycosylation step catalyzed by Golgi alpha-mannosidase II: a QM/MM metadynamics investigation. *J. Am. Chem. Soc. 132*, 8291−8300.
(69) Raiteri, P., Laio, A., Gervasio, F. L., Micheletti, C., and Parrinello, M. (2005) Efficient Reconstruction of Complex Free Energy Landscapes by Multiple Walkers Metadynamic. *J. Phys. Chem. B 110*, 3533−3539.
(70) Hermann, J. C., Hensen, C., Ridder, L., Mulholland, A. J., and Holtje, H.-D. (2005) Mechanisms of antibiotic resistance: QM/MM modeling of the acylation reaction of a class A beta-lactamase with benzylpenicillin. *J. Am. Chem. Soc. 127*, 4454−4465.
(71) Hermann, J. C., Pradon, J., Harvey, J. N., and Mulholland, A. J. (2009) High level QM/MM modeling of the formation of the tetrahedral intermediate in the acylation of wild type and K73A mutant TEM-1 class A beta-lactamase. *J. Phys. Chem. A 113*, 11984−11994.
(72) Acevedo, O., and Jorgensen, W. L. (2009) Advances in Quantum and Molecular Mechanical (QM/MM) Simulations for Organic and Enzymatic Reactions. *Acc. Chem. Res. 43*, 142−151.